Relative dosimetry using active matrix flat-panel imager (AMFPI) technology

Y. El-Mohri,[a] L. E. Antonuk, J. Yorkston,[b] K.-W. Jee, M. Maolinbay, K. L. Lam, and J. H. Siewerdsen[c]
Department of Radiation Oncology, University of Michigan Medical Center, Ann Arbor, Michigan 48109

(Received 21 January 1999; accepted for publication 13 May 1999)

The first examination of the use of active matrix flat-panel arrays for dosimetry in radiotherapy is reported. Such arrays are under widespread development for diagnostic and radiotherapy imaging. In the current study, an array consisting of 512×512 pixels with a pixel pitch of 508 μm giving an area of $26\times26\,cm^2$ has been used. Each pixel consists of a light sensitive amorphous silicon (a-Si:H) photodiode coupled to an a-Si:H thin-film transistor. Data was obtained from the array using a dedicated electronics system allowing real-time data acquisition. In order to examine the potential of such arrays as quality assurance devices for radiotherapy beams, field profile data at photon energies of 6 and 15 MV were obtained as a function of field size and thickness of overlying absorbing material (solid water). Two detection configurations using the array were considered: a configuration (similar to the imaging configuration) in which an overlying phosphor screen is used to convert incident radiation to visible light photons which are detected by the photodiodes; and a configuration without the screen where radiation is directly sensed by the photodiodes. Compared to relative dosimetry data obtained with an ion chamber, data taken using the former configuration exhibited significant differences whereas data obtained using the latter configuration was generally found to be in close agreement. Basic signal properties, which are pertinent to dosimetry, have been investigated through measurements of individual pixel response for fluoroscopic and radiographic array operation. For signal levels acquired within the first 25% of pixel charge capacity, the degree of linear response with dose was found to be better than 99%. The independence of signal on dose rate was demonstrated by means of stability of pixel response over the range of dose rates allowed by the radiation source (80–400 MU/min). Finally, excellent long-term stability in pixel response, extending over a 2 month period, was observed. [S0094-2405(99)02308-1]

Key words: relative dosimetry, active matrix flat-panel imager, electronic portal imager, amorphous silicon, quality assurance

I. INTRODUCTION

In external beam radiotherapy, electronic portal imaging devices (EPIDs) are used for real-time digital acquisition of images prior to and during radiation treatment in order to assist in verifying patient setup. Moveover, in recent years the possibility of using EPIDs for a variety of dosimetric applications has been extensively studied. These studies were performed using two types of EPIDs, video-based systems[1,2] and the liquid filled matrix ion chamber system.[3,4] These studies have shown that such systems can be used as quality control devices for measurement of beam profiles, quality assurance parameters (such as treatment machine output, beam flatness and symmetry), and, ultimately, for measurement of dose delivery (exit dosimetry).

More recently, a new type of EPID, based on the same active matrix flat-panel imager (AMFPI) technology being extensively developed for diagnostic imaging,[5–7] is being introduced to radiotherapy portal imaging.[8–11] Among the various AMFPI designs under consideration for radiotherapy imaging, those employing arrays of amorphous silicon (a-Si:H) thin-film transistors (TFTs) and photodiodes, developed at our institution in collaboration with scientists at Xerox, PARC,[8,12,13,14] have shown considerable promise for improving image quality.[8] It is therefore of interest to investigate the potential of such arrays for dosimetric applications.

The potential use of TFT+photodiode active matrix arrays for dosimetry is particularly interesting given the characteristics and properties of these arrays. For example, the detection area of such arrays can be made relatively large with $30\times40\,cm^2$ arrays recently reported[15] and even larger arrays likely in the near future. Furthermore, the possibility of obtaining dosimetric data over such a large area in a single acquisition is very attractive compared to the tedious acquisition of data using a single, mechanically scanned, ionization chamber. In addition, these arrays are well suited to the high doses associated with the radiation therapy environment as evidenced by previous studies demonstrating that a-Si:H photodiodes and TFTs are radiation damage resistant to very high doses (i.e., $\geqslant10^4$ Gy).[16,17] Also, the ability to acquire dosimetric data digitally and in real-time make the use of active matrix arrays highly attractive when compared to the delays and quality problems associated with film development and scanning. Moreover, with their thin profile, AMFPI detectors can be compactly housed in an enclosure similar to

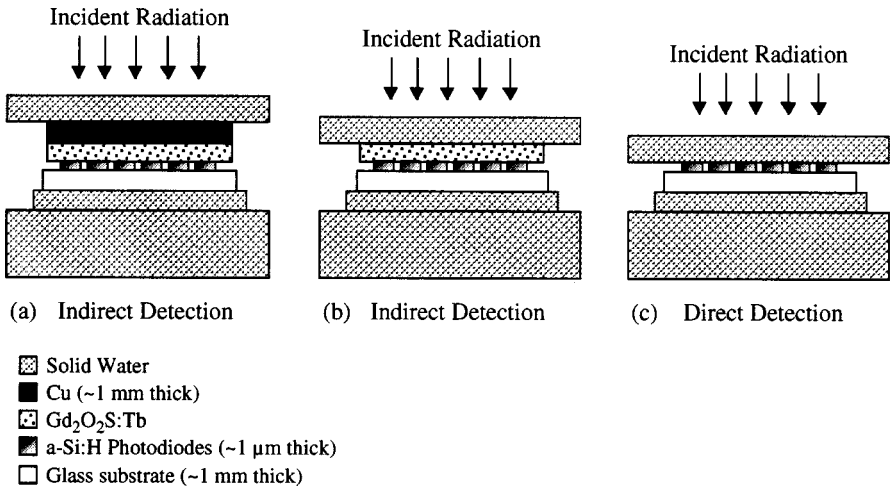

FIG. 1. Illustration of the experimental configurations of the flat-panel detector used in the measurements. The indirect detection configuration uses a phosphor screen with (a) and without (b) an overlying copper plate. The direct detection configuration (c) does not use a phosphor screen or copper plate. The various components shown are not drawn to scale.

a film cassette, presenting minimum restriction to the free movement of a radiation treatment gantry. Finally, these devices are capable of operating both in radiographic mode (corresponding to the capture of a single frame of data following a brief irradiation) as well as in fluoroscopic mode [corresponding to the capture of a continual series of data frames, at up to ~30 frames per second (fps), while the radiation is being delivered].[5] Consequently, it is conceivable that these devices could be employed for dynamic dose distribution measurements in intensity modulated radiation therapy (IMRT), a technique that has received considerable interest in recent times for its potential for achieving high dose and high precision radiotherapy (e.g., see Ref. 18).

With all these qualities and advantages, it is appealing to investigate the feasibility of using AMFPI technology for dosimetry applications. Moreover, recent improvements in a variety of array properties (including reduction of dark current, elimination of dark current drift, improved robustness of the surface passivation, and reduction of pixel and line defects,[5,8] have made an evaluation of the dosimetric potential of this technology practical. In this paper, the possibility of employing TFT+photodiode active matrix arrays for dosimetry is examined through quantitative comparisons of relative dosimetric data acquired with an array and with a conventional ionization chamber. In addition, a variety of pixel properties, relevant to the use of such arrays for dosimetry, are investigated.

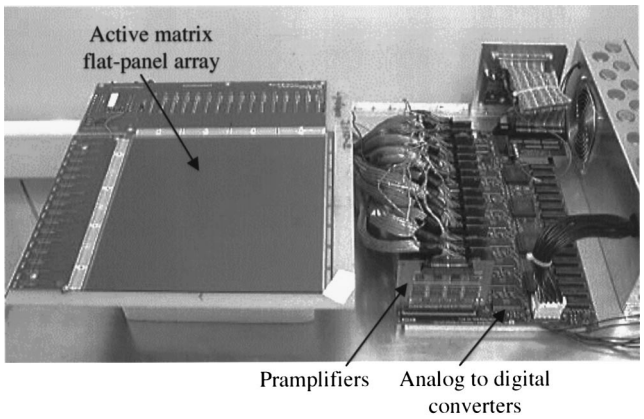

FIG. 2. Photograph of the flat-panel detector and the associated electronic acquisition system.

II. METHODS AND MATERIALS

A. System description

In this paper, the active matrix flat panel detector which was evaluated consists of three main components: an array which incorporates *a*-Si:H TFTs and photodiode pixels deposited on a glass substrate; data acquisition electronics which control the operation of the array and process analog pixel data;[19] and a host computer which controls the acquisition electronics and handles the digital pixel data. For some measurements, a Lanex Fine phosphor screen (Eastman Kodak; ~34 mg/cm^2 Gd_2O_2S:Tb) was placed in contact with the array surface. This screen was used with and without an overlying copper plate (~1 mm thick), as depicted in Figs.

TABLE I. Specifications of the array employed in the flat-pannel detector. The pixel charge capacity is determined at a photodiode reverse bias voltage (V_{bias}) of −5 V (Ref. 8). The maximum frame rate is based on a TFT-on voltage of 10 V, and a pixel sampling time of 5 time constants (Ref. 5). The pixel fill factor is defined as the ratio of the radation sensitive area divided by the total pixel area.

Pixel format (Data×Gate)	512×512
Pixel pitch	508 μm
Array dimensions	26.0 cm×26.0 cm^2
Photodiode geometric area	~0.22 mm^2
Fill factor	~0.84
Nominal photodiode capacitance	~16.9 pF
Pixel charge capacity (V_{bias}=−5 V)	~90 pC
Pixel dark current (V_{bias}=−5 V)	~0.3 pA/mm^2
Maximum frame rate	~22 fps

1(a) and 1(b), respectively. However, for the majority of the measurements, data was acquired without a screen or copper plate, as illustrated in Fig. 1(c). Finally, in order to allow comparisons with data obtained with an ion chamber scanned in a water tank, solid water was positioned above and below the array as shown in Fig. 1. Above the array, the thickness of solid water used varied from 1.5 to 5.0 cm while the thickness below the array was fixed at ~15 cm. A photograph of the array connected to the acquisition electronics appears in Fig. 2.

The array has an active area of $26.0\times26.0\,cm^2$ and consists of a matrix of 512×512 pixels with a pixel pitch of 508 μm. (Detailed specifications of the array are given in Table I.) The pixels along each row are connected to a common Gate address line (Gate line) while the pixels along each column are attached to a common Data address line (Data line). Each pixel consists of a light sensitive photodiode coupled to a thin-film transistor. While the photodiode serves both to sense radiation as well as to store charge (i.e., electron–hole pairs), the TFT acts as a switch enabling the readout of the accumulated charge on a row-by-row basis under the control of the acquisition electronics. Electron–hole pairs generated in the photodiode sensor are collected by means of an electric field established across the sensor by a reverse bias voltage. In the experimental geometries schematically illustrated in Figs. 1(a) and 1(b) employing a phosphor screen (analogous to the configurations used in megavoltage and diagnostic imaging, respectively), dose response of the detector derives primarily from the detection of optical photons which are created in the phosphor by the incident radiation. This will be referred to as the indirect detection configuration in this paper. Alternatively, when no converter is employed (referred to as the direct detection configuration), pixel charge is primarily generated in the photodiode by means of ionizing electrons produced within the solid water overlying the array.

Array readout is performed for one row of pixels at a time by integrating the charge from each pixel in an external charge sensitive preamplifier circuit located at the end of each Data line. Analog signals from the preamplifiers are multiplexed and digitized to 15 bits. Continuing this process until all rows on the array, or some specified number of rows, are addressed constitutes a ''readout cycle.'' When the two-dimensional matrix of pixel values resulting from a readout cycle is saved, this is termed a ''data frame.''

Compared to previous AMFPI systems[8,14,20] which used wirebonds to connect the array to peripheral printed circuit boards (motherboards), the flat-panel detector used in this study employs flexible, printed circuit connectors. These connectors are ''heat-sealed'' both to the periphery of the array and to the motherboard in order to provide electrical contact. Unlike wirebond connections, heat-seal connectors are sufficiently robust and thin to allow the placement of slabs of solid water in close proximity to the array, even when the surface of the solid water extends beyond the edge of the array. In addition, for the purpose of dosimetry measurements, the array was mounted on a piece of solid water, ~1 cm thick, to provide mechanical support and to simulate response in water.

B. General experimental conditions

All measurements were performed using a Clinac-1800 linear accelerator (Varian Associates) using 6 and 15 MV photon beams calibrated such that 1 MU delivers 1 cGy of dose at 100 cm from the source at a depth of d_{max} in water for a $10\times10\,cm^2$ field. (Field sizes are defined at the isocentric distance of 100 cm.) The accelerator delivers the radiation in pulses that are of approximately equal intensity and of ~5 μs duration. For a given dose rate, these pulses are delivered at a fixed frequency, although a feedback mechanism drops pulses as necessary to keep the radiation output constant. Array data were acquired by operating the flat-panel detector in radiographic as well as in fluoroscopic mode.[5] For both modes, the frame time was adjusted in order to vary the dose per frame. (Frame time refers to the period between readout cycles.) In the fluoroscopic mode only a relatively small, contiguous portion of the array (32 Data lines by 6 Gate lines, corresponding to an area of $\sim16.2\times3.0\,mm^2$) was read out. Given that the array continues to receive radiation during fluoroscopic readout, addressing only a portion of the array (which results in shorter frame times) allows the achievement of lower doses per frame. For radiographic mode the portion of the array read out varied depending on the measurement, as noted below. In both cases the selected pixels for which data were analyzed (9 pixels) were representative of correctly functioning pixels. For all measurements, the TFT-on and TFT-off voltages applied to the gate contacts of the pixel TFTs were kept at +10 and -8 V, respectively. The pixel photodiode reverse bias voltage was maintained at -5 V giving a total pixel charge capacity of ~90 pC. The integration time of the preamplifier circuits, which defines the duration of pixel charge integration, was set to 300 μs. This is more than sufficient to accommodate the ~18 μs time constant of the pixels.[5]

C. Synchronization of array readout with the radiation source

For both radiographic and fluoroscopic modes of operation, array readout cycles were synchronized with the radiation source in order to ensure that all rows read out were exposed to the same amount of radiation per data frame. For radiographic mode, synchronization was achieved by means of a trigger/delay pulse generated by the acquisition electronics.[8] The leading edge of this pulse provides a trigger for the radiation and is issued following the final initializing cycle, as shown in Fig. 3(a). The trailing edge of the pulse provides a trigger for the start of the next readout cycle which provides the data frame. The width of this pulse is adjusted (under software control) so as to accommodate the duration of the irradiation. The initialization cycles performed prior to the irradiation serve to remove trapped charge that accumulates in the photodiodes when the detector is not being read out.

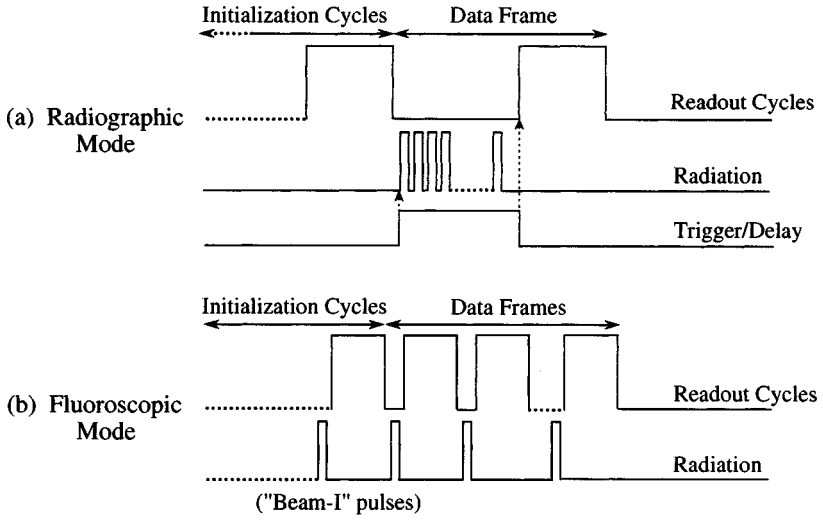

FIG. 3. Timing diagram illustrating the synchronization of array readout with radiation beam delivery for (a) radiographic and (b) fluoroscopic operation.

For fluoroscopic operation, synchronization of array readout with the radiation was achieved by means of pulses (''Beam-I'') supplied by the linear accelerator. These pulses coincide with the radiation pulses and are used to trigger the next readout cycle. The readout speed of the acquisition electronics is sufficient to insure that the entire data frame (consisting of six rows of pixels) can be acquired between consecutive radiation pulses. The number of radiation pulses prior to each data frame was varied from 1 [corresponding to the case illustrated in Fig. 3(b)] to 900 thereby allowing the dose per frame to be varied (from ~0.027 to ~24 MU). Finally, initialization of the array consisted of performing 50 readout cycles (with radiation ''on'') prior to capture of the first data frame so as to ensure that charge trapping and charge release are at equilibrium.[5]

D. Linearity of response and dose rate dependence

It is highly desirable that the signal response of a dosimeter be linear with dose and exhibits no dependence on dose rate as this minimizes the degree to which the data needs to be corrected in order to allow straightforward interpretation. For the indirect detection configuration, it is reasonable to assume that these conditions are satisfied given that: (a) earlier studies have already demonstrated that the optical response of pixels from the 508 μm pitch arrays exhibits highly linear response up to ~30% (~75%) of the pixel signal capacity for radiographic (fluoroscopic) mode;[8] and (b) dose rate independence can be inferred from previously reported reciprocity x-ray measurements involving a 450 μm pitch array of similar design which was coupled to a phosphor screen.[21] In order to verify that linearity and dose rate independence are also satisfied for the direct detection configuration, measurements were performed at 6 MV for accelerator dose rates of 80, 160, 240, 320, and 400 MU/min up to ~25% of the pixel signal capacity. In these measurements, the detector was positioned at a source-to-detector distance (SDD) of 101.5 cm, at d_{max} (1.5 cm), and with a field size of $10\times10\,cm^2$. Data were acquired for both fluoroscopic and radiographic mode with the dose per data frame ranging from 1 to ~25 MU. For both modes, a total of 6 Gate lines and 32 Data lines were addressed. In the case of radiographic operation, the frame time was varied from ~0.15 s to ~7.8 s so as to accommodate the time for delivery of the radiation. In this case, the radiographic initialization time (which corresponds to the duration of array readout in the dark immediately prior to irradiation[5]) was fixed at ~62 s. The use of a constant radiographic initialization time is important in insuring constancy in pixel response. For fluoroscopic mode the frame time was varied from ~0.25 s to ~12 s, depending on the frequency and number of radiation pulses required per frame. For each frame time, a pair of measurements were performed: one in dark and another with radiation. For a given pixel, the difference between these two measurements (corresponding to the pixel response) was examined as a function of dose and dose rate.

E. Sensitivity

The dosimetry measurements in this paper were acquired under conditions of highly linear pixel response. This was accomplished by operating the detector at signal levels where the pixel response was either known (for indirect detection)[8] or determined (for direct detection) to be highly linear in both radiographic and fluoroscopic modes. Given the known charge capacity of the pixels (Table I), this required a knowledge of the sensitivity of the detector (i.e., signal response per unit incident radiation) for the various detector configurations (Fig. 1). Sensitivity data were acquired at 6 and 15 MV using a field size of $10\times10\,cm^2$, a SDD of 100 cm and a thickness d_{max} of solid water overlying the array. The detector was operated in fluoroscopic mode for frame times ranging from ~40 ms to ~2.8 s. The measurement technique consisted of determining the pixel response by acquiring signal data as a function of dose. In addition, data in the absence of radiation was also acquired and subtracted from the measured pixel response data. A linear fit to the corrected pixel response data was performed, and the resulting slopes for all pixels were averaged to yield the sensitivity in units of pC/cGy/pixel.

F. Long and short term reproducibility

For arrays of the design examined in this paper, short term stability (over hours of operation) has been previously demonstrated.[8] Specifically, dark signal variations were of the same magnitude as the noise fluctuations inherent to the system. In order to explore longer term signal variations, which affect the practicality of the detector, measurements were performed over a period of ~2 months using the direct detection configuration. Data was acquired using a 6 MV photon beam, for a $10\times10\,\mathrm{cm}^2$ field size, at a SDD of 101.5 cm, at $d_{\max}$. The array was operated in radiographic mode at a dose per frame of 10 MU and at a dose rate of 320 MU/min. The portion of the array addressed consisted of a block of 32×6 (Data×Gate) pixels. The frame time was set to ~2.7 s and the radiographic initialization time was ~80 s.

G. Field profile measurements

In order to test the relative dosimetry capabilities of the flat-panel detector, a series of data frames were acquired for various field sizes. Due to the limited active area of the flat-panel detector ($26\times26\,\mathrm{cm}^2$), data for field sizes up to $20\times20\,\mathrm{cm}^2$ were taken. The data frames (consisting of 512×512 pixels) were acquired in radiographic mode at 6 and 15 MV for the detector configurations shown in Fig. 1. In order to maintain signal sizes within the linear range of pixel response, and given the difference in sensitivity between the direct and indirect detection configurations, the dose per frame was 1 and 10 MU, respectively. For each data frame taken with the radiation ''on,'' a dark frame, obtained under the same conditions but with the radiation ''off,'' was acquired and subtracted. In this way, fluctuations primarily due to channel-to-channel variations in preamplifier signal offset and partially due to pixel-to-pixel differences in pixel dark current were largely reduced. No correction for pixel-to-pixel gain variations was performed on the data. The resulting data can then be displayed in various ways, including the extraction of one-dimensional profiles in any direction at any position within the radiation field. In the present measurements, beam profiles along the center of the field were extracted. This direction corresponded to extracting data from individual Data lines on the flat-panel detector. For comparison with the flat-panel data, beam profiles along the center of the field were obtained with a commercial ion chamber scanning system (Welhoffer, Dosimetrie, Germany) using a cylindrical chamber (IC10) with an inner diameter of ~6 mm. The ion chamber was immersed in a $45\times45\times45\,\mathrm{cm}^3$ water tank and scans were performed in a continuous fashion across the field while the accelerator was delivering the radiation. An additional ion chamber was used to monitor the beam in order to correct for fluctuations in accelerator output. For all data showing one-dimensional beam profiles central field normalization was applied. The distance from the source to the surface of the buildup material (solid water or water in the case of the array and ion chamber measurements, respectively, of thickness, d) (SSD) was fixed at 100 cm.

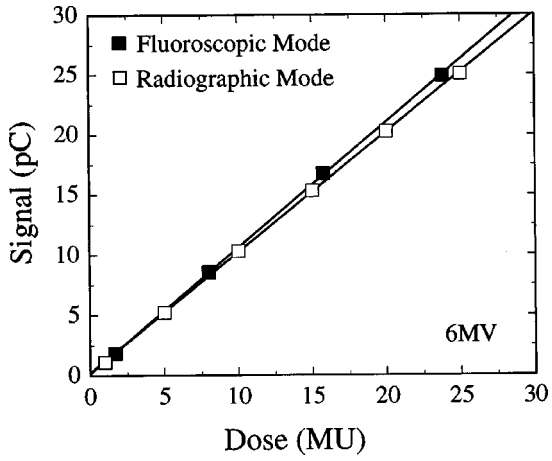

FIG. 4. Pixel response as a function of dose for two modes of array operation (radiographic and fluoroscopic). The data were acquired at 6 MV using the direct detection configuration. For the pixel data shown in this figure, and in the following figures, the dark signal component has been subtracted. Each line corresponds to a least squares fit of the data.

III. RESULTS

A. Linearity of response and dose rate dependence

Figure 4 shows the measured pixel response as a function of dose for radiographic and fluoroscopic modes for the direct detection configuration. Highly linear response is observed throughout the signal range considered (the first ~25% of pixel charge storage capacity), in line with more extensive linearity studies performed with an array of similar design.[8] The small reduction in detector response observed for radiographic mode is probably due to charge loss caused by charge trapping in metastable states of the a-Si:H.[5,8] Fluoroscopic mode, on the other hand, does not suffer from this loss since equilibrium is always established between charge trapping and release.[5]

Figure 5 shows pixel response as a function of dose rate

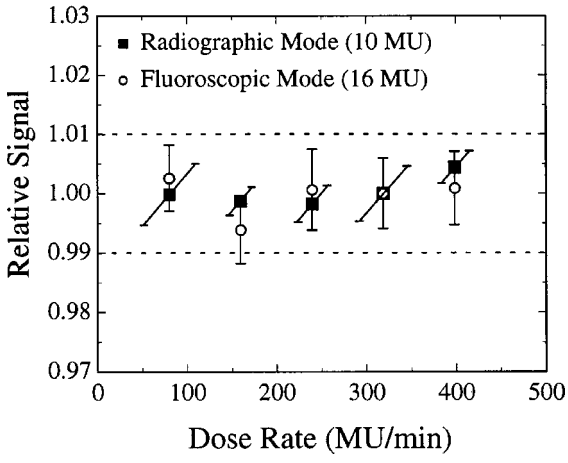

FIG. 5. Relative pixel response as a function of dose rate for radiographic and fluoroscopic mode. The data was acquired at 6 MV using the direct detection configuration. The dashed lines indicate deviations of ±1% from unity. The uncertainties in the measurements are indicated by error bars with the bars for the radiographic data drawn obliquely for reasons of clarity. See text for details.

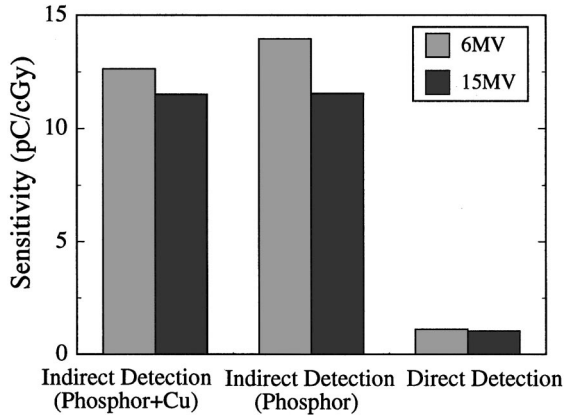

FIG. 6. Pixel sensitivity for the various detection configurations at 6 and 15 MV.

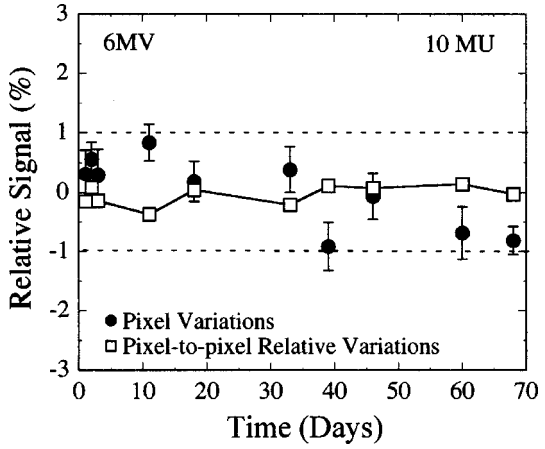

FIG. 7. Pixel response as a function of elapsed time. The data was acquired at 6 MV using the direct detection configuration. The solid circles correspond to measured data from a single pixel divided by the average response over the entire measurement period. The open squares represent the ratio of responses for a pair of pixels, divided by the average value of this ratio over the entire period.

of the accelerator for both modes using the direct detection configuration. The dose per frame was set to 10 and 16 MU for radiographic and fluoroscopic mode, respectively. For each mode, each data point corresponds to the measured pixel response at that dose rate divided by the average response for all dose rates. The error bars are relatively small ($\pm 1\%$) and represent standard deviations in the mean pixel response over 20 consecutive samples. From the data presented in the figure and within the margin of error indicated, detector response is seen to be independent of dose rate.

B. Sensitivity

Sensitivity data were acquired for signal values ranging up to $\sim$20% of pixel charge capacity, where the pixel response is known to be highly linear as detailed above. The results are shown in Fig. 6 for the indirect and direct detection configurations. For the direct detection configuration, the sensitivity is over an order of magnitude smaller than the results for the indirect detection configuration (e.g., $\sim$1.1 pC/cGy/pixel at 6 MV). This is a consequence of the reduced gain offered by the ~ 1 μm thick photodiode of the direct detection compared to that offered by the phosphor (or phosphor+copper) of the indirect detection. In addition, for indirect detection the sensitivities are systematically higher at 6 MV than 15 MV. This is probably due to the increased probability of interaction of the primary radiation with the phosphor (or phosphor+copper combination) at 6 MV. The slightly enhanced sensitivities observed for the indirect detection configuration using phosphor+copper compared to the configuration using phosphor only is due to the reduction in dose when copper is added, a configuration corresponding to increased equivalent water depth ($>d_{\max}$).

C. Long term reproducibility

The variation of pixel response over a $\sim$2 month period is shown in Fig. 7. In the figure, the solid circles correspond to measured pixel response divided by the average response over the entire period. For each data point, the error bars represent standard deviations in the mean pixel response over 20 consecutive samples. Over the measurement period, the results varied by a maximum of $\pm 1\%$ (dashed horizontal lines) most likely due to fluctuations in accelerator output. In order to illustrate pixel-to-pixel variations over the same time period, the relative response of two pixels divided by the average relative response of these pixels over the entire period is also shown in Fig. 7 (open squares). In this case, since fluctuations in the accelerator output equally affect both pixels, the long term variation in relative pixel response is smaller (less than $\pm 0.4\%$). These results demonstrate excellent stability of the response of the flat-panel detector both in absolute and relative terms.

D. Field profile measurements

Figures 8(a) and 8(b) show sample plots corresponding to a frame of data acquired at 6 MV for a field size of $15 \times 15\,\mathrm{cm}^2$ using the direct detection configuration. In order to better illustrate the results, the number of data points in Fig. 8(a) have been reduced by a factor of 10 in regions of flat dose response and the distracting influence of pixel and line defects have been removed through application of a selective median filter. A careful examination of the data reveals a lower degree of signal fluctuations along the Data lines compared to the Gate lines. The origin of this difference arises from the fact that pixels along a Data line have their signal sampled by the same preamplifier, while pixels along a Gate line are connected to separate preamplifiers. Therefore, the larger pixel-to-pixel signal fluctuations along the Gate lines (including the anomalous peak on the left) may be attributed to channel-to-channel variations in the preamplifier gains. (Signal fluctuations arising from channel-to-channel variations in preamplifier offset and pixel-to-pixel dark current differences are removed by the dark frame subtraction.) Figure 8(b) illustrates the data in the form of a contour plot where each contour represents a constant pixel value, normalized to the maximum value in the data set. The parallel islands observed running along the Data lines in the central

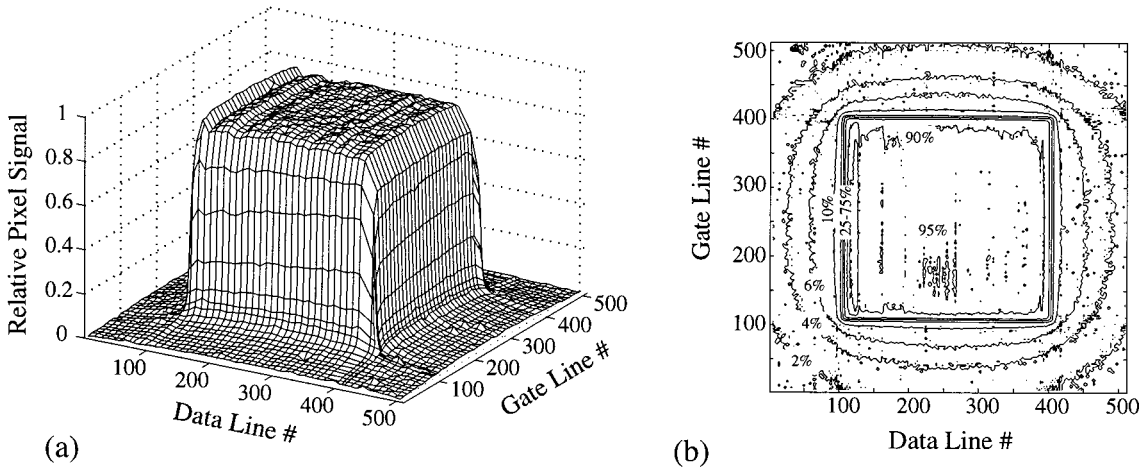

FIG. 8. (a) Surface plot of a single frame of data from the flat-panel detector using the direct detection configuration. The data were taken at 6 MV and 15 $\times 15\ \mathrm{cm}^2$ field with 1.5 cm of solid water overlying the array. (b) Two-dimensional contour plot of the same frame of data.

region where the radiation field is expected to be relatively flat are also a result of the channel-to-channel variations in preamplifier gain.

Figures 9(a) and 9(b) show field profiles obtained at 6 and 15 MV, respectively, for a $15\times 15\ \mathrm{cm}^2$ field using both the direct detection configuration and the indirect detection configuration employing the phosphor+copper combination. (Results for the configuration using the phosphor alone were practically indistinguishable from that of the phosphor+copper combination and thus are not shown.) For each configuration, the data presented corresponds to that obtained from a single Data line, that line which most closely traversed the center of the radiation field for the given experimental setup. The small number of sporadically-positioned data points exhibiting low signal response correspond to defective pixels. In order to remove the distracting effect of such pixels, their corresponding data points have been removed in subsequent figures. For comparison, data acquired with an ion chamber under equivalent irradiation conditions are also shown in each figure in the form of a continuous line. At 6 MV [Fig. 9(a)], large differences are observed between the indirect detection data and the ion chamber data, up to ~7% lower relative response inside the field boundaries and up to ~13% higher response outside.

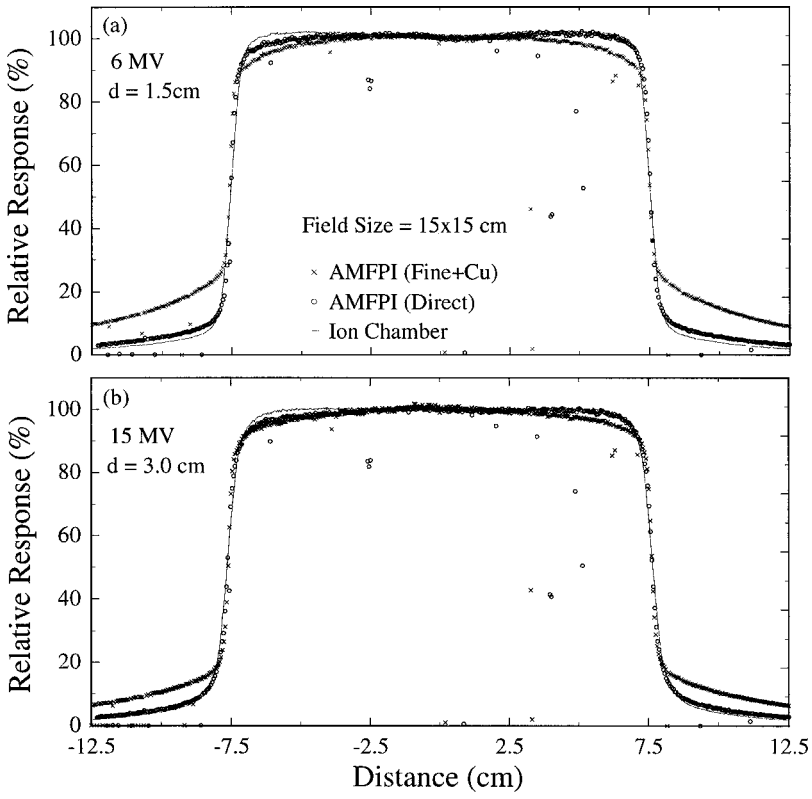

FIG. 9. Field profiles obtained with the flat-panel detector using the direct detection configuration (circles) and the indirect detection configuration (crosses). For comparison, data from a standard ion chamber system is shown in the form of lines which represent interpolations between data points. Data were taken with a $15\times 15\ \mathrm{cm}^2$ field (a) at 6 MV at a depth of ~1.5 cm; and (b) at 15 MV at a depth of ~3 cm. The material overlying the detector was solid water for the flat-panel device and water for the ion chamber. For each beam energy, the depth of overlying material used correponds to the depth of maximum dose ($d_{\max}$) in water.

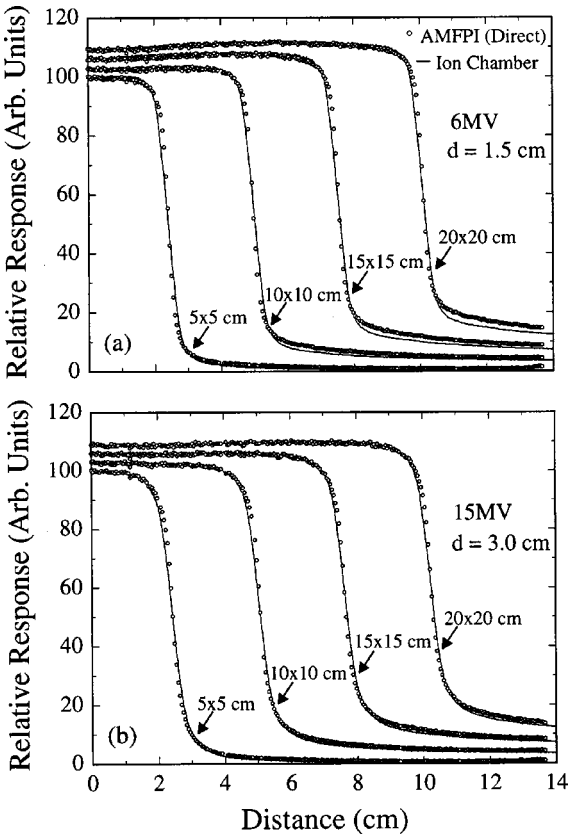

FIG. 10. Field profiles obtained with the flat-panel detector using the direct detection configuration (circles) for various field sizes (5×5, 10×10, 15×15, and 20×20 cm^2). For comparison, data from an ion chamber system is also shown (lines). As in the case of Fig. 9, the data were obtained (a) at 6 MV with 1.5 cm of overlying material, and (b) at 15 MV with 3.0 cm of overlying material.

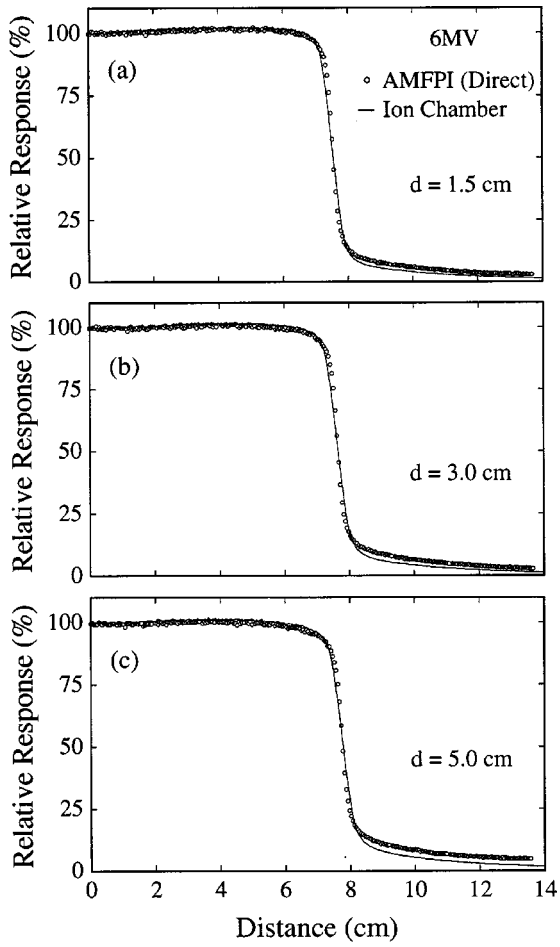

FIG. 11. Field profiles obtained with the flat-panel detector at 6 MV using the direct detection configuration (circles) at depths of (a) 1.5 cm, (b) 3.0 cm, and (c) 5.0 cm. These data are compared to data obtained from an ion chamber system (lines).

These differences are probably due to the relatively higher signal response of the phosphor screen to the low energy scatter component of the radiation[22] (as compared to ion chamber response). Compared to an air-filled ion chamber, the higher average atomic number and density of the indirect detector ($Z_{\text{eff}}\cong60$ for Gd_2O_2S:Tb) leads to a detector response which is more strongly dependent on the energy of the radiation interacting in the detector. By comparison, the direct detection profiles are in reasonable agreement with the ion chamber data (differences are mostly within ~1% inside the field boundaries), as seen in Fig. 9(a). This is a direct result of the fact that the detector (i.e., the photodiode, mainly containing silicon, $Z_{\text{eff}}\cong14$) is very thin (~1 μm) and that its response, which depends on the ratio of the restricted mass stopping powers of silicon and water, is approximately independent of energy (~7% variations for 0.1–6 MeV electrons energy range[23]). The greater degree of disagreement between the direct detection and ion chamber data on the left shoulder (~4%) was found to be directly related to a specific region of the array. Since this discrepancy is only observed in the direct detection configuration and is small, it is believed to originate from nonuniformities in the thickness of the *a*-Si:H photodiodes leading to pixel-to-pixel gain differences. In the case of the indirect detection

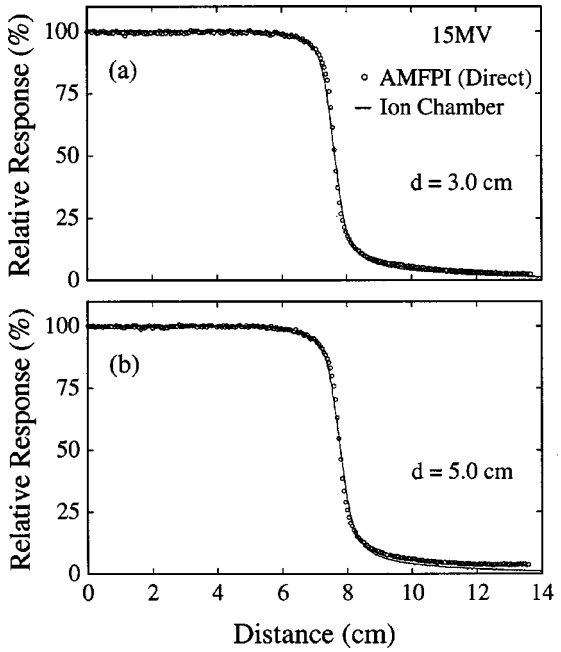

FIG. 12. Field profile plots obtained with the flat-panel detector at 15 MV beam using the direct detection configuration (circles) at various dose depths [(a) 3.0 and (b) 5.0 cm] and compared to those from an ion chamber system (lines).

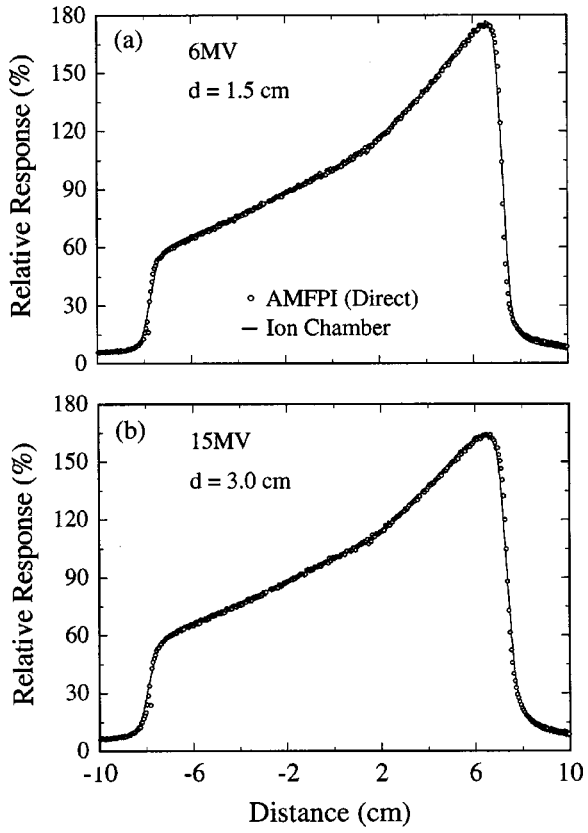

FIG. 13. Field profile plots obtained with the flat-panel detector using a 60° wedge and $15\times15\ \text{cm}^2$ radiation field (circles) at (a) 6 MV, and (b) 15 MV, and compared to those from an ion chamber system (lines).

configuration, these nonuniformities will not affect pixel gain since optical photons generated in the phosphor interact within a short distance in the photodiode. The slightly enhanced response of the direct detection configuration compared to the ion chamber outside the field boundaries, which is more pronounced for the lower energy beam, is possibly due to backscatter contributions from the array substrate.[24]

In the case of the 15 MV beam profile data shown in Fig. 9(b), the differences between the response of the flat-panel detector and that of the ion chamber are less pronounced than at 6 MV, particularly outside the field boundaries. At 15 MV, the higher energy beam results in a higher energy scatter component, which in turn leads to a lower probability of interaction and therefore to a less enhanced flat-panel detector response (as compared to the 6 MV beam). As in the case for 6 MV, at 15 MV the results for the direct detection configuration are in reasonable agreement with those from the ion chamber. At both 6 and 15 MV, small differences in the slope of the flat-panel and ion chamber data are observed at the field edges. These differences are a consequence of the higher spatial resolution provided by the flat-panel detector, a 0.5 mm pixel pitch compared to a 6 mm inner diameter for the ion chamber, leading to better field edge definition.

In Figs. 10–13, flat-panel detector results corresponding to field profiles obtained using the indirect detection configuration are not shown. In Figs. 10(a) and 10(b), profiles obtained at 6 and 15 MV for various field sizes are shown along with results obtained with the ion chamber system. For clarity of presentation, only half-field profiles are shown, and for each field size a common arbitrary offset was applied to the flat-panel and ion chamber data in the vertical direction. As illustrated in the figures, good agreement between the flat-panel and ion chamber data is observed within the radiation field for all field sizes (differences are within ~1%). For all locations on the radiation field, the absolute response obtained with the direct detection configuration and with the ion chamber increases with field size, due to the increase in scattered radiation. Consequently, outside the field boundary, the absolute magnitude of the difference between the two normalized responses (ion chamber vs flat-panel detector) also increases, as is evident in the figure, particularly for the 6 MV case.

Figures 11 and 12 show half-field profiles measured with various thicknesses of material overlying the detector. The results were obtained at 6 MV and 15 MV, respectively, using a $15\times15\ \text{cm}^2$ field size. For both beam energies, reasonable agreement is obtained between the flat-panel detector and ion chamber within the radiation field (differences are within ~1%). Outside the field boundary, as the thickness of the overlying material increases, larger discrepancies between the flat-panel detector and the ion chamber data are observed.

Finally, Figs. 13(a) and 13(b) show profiles obtained at 6 MV and 15 MV, respectively, using a $15\times15\ \text{cm}^2$ field size, at a depth of $d_{\max}$, and with a 60° wedge. Reasonable agreement is once again observed between the flat-panel detector and the ion chamber system. On the left shoulder of the profile, the flat-panel detector exhibits the same response drop observed in Fig. 9 (up to ~4%).

IV. DISCUSSION AND CONCLUSIONS

Since the initial conception of an indirect-detection, active matrix flat-panel detector for radiotherapy imaging,[12] tremendous progress has taken place in array design and fabrication. This has led to increased array size, improved signal characteristics, and fewer array defects. For example, continual incremental improvements to the fabrication process have allowed the realization of progressively larger areas and higher fill factor resulting in the $26\times26\ \text{cm}^2$, 508 μm pitch, ~84% fill factor array used in this paper. Furthermore, the incorporation of a scratch-resistant, nonhygroscopic passivation layer (oxynitride) in this array resulted in considerably more stable operation.[8] Such improvements have facilitated the examination of the possible use of this technology for a variety of applications in radiotherapy. Previous studies using this array have demonstrated its strong potential for high quality, low dose portal localization and verification imaging[8] and led to the recent implementation of this array design in a clinical environment.[10] In the present paper, this array has been employed to perform an initial examination of the application of AMFPI technology to relative dosimetry. Measurements were performed both in radiographic and fluoroscopic modes with array operation synchronized with 6 and 15 MV radiation delivered from a therapy linear accel-

erator. Data were acquired for a variety of field sizes and depths of overlying absorbing material, with and without wedges.

The performance of an active matrix flat-panel detector as a relative dosimeter has been studied for two configurations; an indirect detection configuration where the detector senses the incident radiation via an overlying Lanex Fine phosphor screen with and without an overlying copper plate (analogous to configurations used in imaging); and a direct detection configuration with no phosphor or copper, for which incident radiation, mainly electrons, interact directly with the thin amorphous silicon layer of the array. The reduced sensitivity exhibited by the direct detection configuration necessitates the delivery of a factor of ~10 times more dose in order to achieve a signal response equivalent to that of the indirect detection configuration. For relative dosimetry, radiation field profiles using both configurations were obtained and compared to ion chamber data acquired under similar dosimetric conditions. Indirect detection exhibits large differences compared to ion chamber data at field edges due to an over-response of the phosphor to low energy scattered radiation. Direct detection produces data more closely replicating that from the ion chamber; however, it is more prone to nonuniform pixel response caused by spatial nonuniformities in photodiode thickness across the array. In the present study, field profile data demonstrate that direct detection provides an accurate measure of beam flatness (within 1% of that obtained from an ion chamber) for various radiation field sizes and overlying absorber thicknesses. Outside the field boundaries, however, the direct detection configuration yields an over-response that could originate from additional signal contributions from radiation scatter from the glass substrate. In addition to a more accurate replication of the ion chamber response, the basic signal characteristics of the direct detection configuration, including linearity of pixel response, dose rate independence, and temporal stability, indicate that such a detector is a strong candidate for performing practical and reliable relative dose measurements.

In order to extract accurate dosimetry data from the total active area of a flat-panel detector, it is necessary to apply a calibration procedure for correcting pixel-to-pixel gain and offset variations. While these variations are in part due to inherent differences in intrinsic pixel-to-pixel response, they also arise from differences in channel-to-channel preamplifier response. In the present study, only an offset correction, applied by means of a dark frame subtraction, was used. As a consequence, the field profiles shown correspond to pixel data extracted along Data lines (as opposed to Gate lines) so as to circumvent channel-to-channel preamplifier gain differences. In order to obtain both gain and offset corrections, several other calibration methods are possible. For example, a limited calibration, which would only correct for the response differences of the various preamplifiers, could be achieved through the direct injection of a known amount of electronic charge to the preamplifier circuits. A more comprehensive calibration, which would correct for both intrinsic pixel and preamplifier response differences, could be performed using a spatially uniform radiation source (''flat-field'' correction[25]). For each detector configuration (indirect or direct), such a calibration can correct for the various factors affecting gain differences across the array including preamplifier circuits (direct and indirect); phosphor light output (indirect only); photodiode quantum efficiency (direct and indirect); and photodiode thickness (direct only).

Flat-panel detectors of the type examined in this paper are capable of operating both in fluoroscopic and radiographic modes. While radiographic operation allows the acquisition of an entire plane of data following a single interval of radiation exposure (unlike a single ion chamber, which requires mechanical scanning and the use of an additional radiation monitor), the corresponding detector response suffers from the effects of charge trapping in the amorphous silicon. These effects lead to the reduction of both the radiation sensitivity and the range of linear response. In the present study, to ensure accurate relative dose measurements, the range of pixel signal was restricted to a region of highly linear response. Alternatively, to make use of the full signal range offered by the pixels, it is conceivable to correct for the nonlinearities observed at larger signal sizes. Fluoroscopic operation, on the other hand, offers a considerably larger range of linear response and no charge trapping effects as long as an equilibrium is established between charge trapping and release in a repeated sequence of measurements (as was the case in all the present measurements). This technique is appropriate for static dose measurements. For the case of dynamic dose measurements (e.g., for an intensity modulated beam), fluoroscopic operation can again be appropriate provided that charge trapping effects are minimized. Without such minimization, charge trapping and release translates into charge carryover between consecutive frames of data, thereby degrading the ability of the system to accurately monitor temporal beam variations. (The magnitude of the charge carryover for high quality arrays is typically ~5%.[5]) Fluoroscopic operation can therefore provide, for example, verification of dynamic multileaf collimator movement in real time, similar to that achieved using other fluoroscopic video-based EPIDs.[26,27] For this application, which would involve the readout of large blocks of pixels, data acquisition speeds considerably higher than that provided by the present acquisition electronics (ideally limited only by the maximum speed imposed by the time constant of the pixels) are necessary. Toward achieving this goal, a new acquisition electronics system allowing well over 30 fps (for a 512×512 pixel array) has been constructed[28] and will allow future investigations into the use of active matrix flat-panel arrays as quality assurance devices for IMRT.

Considering the large discrepancies in relative dose response between the flat-panel detector, employing the indirect detection configuration, and the ion chamber, it would appear difficult for an indirect detection AMFPI for radiotherapy to also provide reasonably accurate patient dose verification. (By comparison, the liquid ionization chamber EPID does appear to offer both imaging and accurate patient dosimetry capabilities.[1,4]) Since the indirect detection AMFPIs thus far evaluated for radiotherapy imaging have employed a phosphor screen (Gd_2O_2S:Tb) to achieve efficient

use of the incident radiation,[8,9] such devices are expected to exhibit dose response characteristics that are not tissue equivalent and therefore do not provide straightforward dose measurements. Similar restrictions are encountered with video-based EPIDs employing a similar phosphor screen. For video-based EPIDs, however, a relatively complex calibration procedure has been devised which provides accurate portal dose measurements.[29] Therefore, we anticipate that similar calibration procedures could be developed to allow indirect detection AMFPIs to provide portal dose measurements. Furthermore, it is conceivable that this would involve even fewer corrections than for video-based EPIDs whose performance is complicated by a variety of factors including glare.[29]

As a system used solely for dosimetry, a photodiode-based, active matrix imaging array used in the direct detection configuration (i.e., without the use of a phosphor) can provide accurate beam quality assurance checks. Alternatively, the use of such an array in conjunction with a scintillator with water-equivalent properties, such as a plastic-based scintillator,[30,31] could potentially provide a dosimetry device offering considerably higher sensitivity than the direct detection configuration.

ACKNOWLEDGMENTS

The authors extend their sincere gratitude to Henry Schek III for assistance with the measurements and data analysis and to Benedick A. Fraass for his encouragement and support. This work is supported by Grant R01-CA51397 from the National Institutes of Health. This work was first presented at the 1996 AAPM annual meeting

[a]Phone: 313-936-4309; Fax: 313-936-7859; electronic mail: elmohri@umich.edu
[b]Present address: Eastman Kodak Company, Health Imaging Research Laboratory, Rochester, New York 14653.
[c]Present address: Department of Radiation Oncology, William Beaumont Hospital, Royal Oak, Michigan 48073.

[1]M. Kirby and P. C. Williams, ''The use of an electronic portal imaging device for exit dosimetry and quality control measurements,'' Int. J. Radiat. Oncol. Biol. Phys. **31**, 593–603 (1995).
[2]B. J. Heijmen, K. L. Pasma, M. Kroonwijk, V. G. M. Althof, J. C. J. de Boer, A. G. Visser, and H. Huizenga, ''Portal dose measurement in radiotherapy using an electronic portal imaging device (EPID),'' Phys. Med. Biol. **40**, 1943–1955 (1995).
[3]R. Boellard, M. van Herk, and B. J. Mijnheer, ''The dose response relationship of a liquid-filled electronic portal imaging device,'' Med. Phys. **23**, 1601–1611 (1996).
[4]Y. Zhu, X-Q. Jiang, and J. Van Dyk, ''Portal dosimetry using a liquid ion chamber matrix: Dose response studies,'' Med. Phys. **22**, 1101–1106 (1995).
[5]L. E. Antonuk, Y. El-Mohri, J. H. Siewerdsen, J. Yorkston, W. Huang, V. E. Scarpine, and R. A. Street, ''Empirical investigation of the signal performance of a high-resolution, indirect detection, active matrix flat-panel imager (AMFPI) for fluoroscopic and radiographic operation,'' Med. Phys. **24**, 51–70 (1997).
[6]J. H. Siewerdsen, L. E. Antonuk, Y. El-Mohri, J. Yorkston, W. Huang, J. M. Boudry, and I. A. Cunningham, ''Empirical and theoretical investigation of the noise performance of indirect detection, active matrix flat-panel imagers (AMFPIs) for diagnostic radiology,'' Med. Phys. **24**, 71–89 (1997).
[7]W. Zhao, I. Belvis, S. Germann, J. A. Rowlands, D. Waechter, and Z. Huang, ''Digital radiology using active matrix readout of amorphous selenium: Construction and evaluation of a prototype real-time detector,'' Med. Phys. **24**, 1834–1843 (1997).
[8]L. E. Antonuk, Y. El-Mohri, J. Yorkston, K. W. Jee, J. Siewerdsen, M. Maolinbay, V. E. Scarpine, and H. Sandler, ''Initial performance evaluation of an indirect-detection, active-matrix flat-panel imager (AMFPI) prototype for megavoltage imaging,'' Int. J. Radiat. Oncol., Biol., Phys. **42**, 437–454 (1998).
[9]P. Munro and D. C. Bouius, ''X-ray quantum limited portal imaging using amorphous silicon flat-panel arrays,'' Med. Phys. **25**, 689–702 (1998).
[10]Y. El-Mohri, L. E. Antonuk, K-W. Jee. K. Brock, J. Balter, K. Lam, D. L. McShan, and B. A. Fraass, ''Initial performance evaluation of a clinical prototype active-matrix flat-panel imager for radiotherapy imaging,'' Med. Phys. **25**, 1583 (1998) (Abstract).
[11]T. Falco, H. Wang, and B. G. Fallone, ''Preliminary study of a metal/a-Si-based portal detector,'' Med. Phys. **25**, 814–823 (1998).
[12]L. E. Antonuk, J. Yorkston, J. Boudry, M. J. Longo, and J. Jimenez, ''Development of hydrogenated amorphous silicon sensors for high energy photon radiotherapy imaging,'' IEEE Trans. Nucl. Sci. **37**, 165–170 (1990).
[13]L. E. Antonuk, J. Boudry, W. Huang, D. L. McShan, E. J. Morton, J. Yorkston, M. J. Longo, and R. A. Street, ''Demonstration of megavoltage and diagnostic x-ray imaging with hydrogenated amorphous silicon arrays,'' Med. Phys. **19**, 1455–1466 (1992).
[14]L. E. Antonuk, J. Yorkston, W. Huang, H. Sandler, J. H. Siewerdsen, and Y. El-Mohri, ''Megavoltage imaging with a large area, flat-panel, amorphous silicon imager,'' Int. J. Radiat. Oncol., Biol., Phys. **36**, 661–672 (1996).
[15]R. A. Street, R. B. Apte, S. E. Ready, R. L. Weisfield, and P. Nylen, ''Amorphous silicon sensor arrays for x-ray and document imaging,'' Mater. Res. Soc. Symp. Proc. **487**, 399–410 (1997).
[16]J. M. Boudry and L. E. Antonuk, ''Radiation damage of amorphous silicon photodiode sensors,'' IEEE Trans. Nucl. Sci. **41**, 703–707 (1994).
[17]J. M. Boudry and L. E. Antonuk, ''Radiation damage of amorphous silicon, thin-film, filed-effect transistors,'' Med. Phys. **23**, 743–754 (1996).
[18]D. J. Convery and M. E. Rosenbloom, ''The generation of intensity-modulated fields for conformal radiotherapy by dynamic collimation,'' Phys. Med. Biol. **37**, 1359–1374 (1992).
[19]E. J. Morton, L. E. Antonuk, J. E. Berry, W. Huang, P. Mody, and J. Yorkston, ''A data acquisition system for flat-panel imaging arrays,'' IEEE Trans. Nucl. Sci. **41**, 1150–1154 (1994).
[20]L. E. Antonuk, J. M. Boudry, Y. El-Mohri, W. Huang, J. H. Siewerdsen, J. Yorkston, and R. A. Street ''Large area, flat-panel amorphous silicon imagers,'' Proc. SPIE **2431**, 216–227 (1995).
[21]L. E. Antonuk, J. H. Siewerdsen, J. Yorkston, and W. Huang, ''Radiation response of amorphous silicon imaging arrays at diagnostic energies,'' IEEE Trans. Nucl. Sci. **41**, 1500–1505 (1994).
[22]H.-P. Chan and K. Doi, ''Studies of x-ray energy absorption and quantum noise properties of x-ray screens by use of Monte Carlo simulation,'' Med. Phys. **11**, 37–46 (1984).
[23]Report 35 of the International Commission on Radiation Units and Measurements, ''Radiation dosimetry: Electron beams with energies between 1 and 50 MeV,'' 1984, pp. 6–7.
[24]J. Yorkston, L. E. Antonuk, Y. El-Mohri, K-W. Jee, W. Huang, M. Maolinbay, X. Rong, and J. H. Siewerdsen, ''Improved spatial resolution in flat-panel imaging systems,'' Proc. SPIE **3336**, 556–563 (1998).
[25]J. A. Seibert, J. M. Boone, and K. Linfords, ''Flat-field correction technique for digital detectors,'' Medical Imaging 1998: Physics of Medical Imaging, SPIE **3336**, 348–354 (1998).
[26]L. Ma, P. B. Geis, and A. L. Boyer, ''Quality assurance for dynamic multileaf collimator modulated fields using a fast beam imaging system,'' Med. Phys. **24**, 1213–1220 (1997).
[27]M. Partridge, P. Evans, A. Mosleh-Shirazi, and D. Convery, ''Independent verification using portal imaging of intensity-modulated beam delivery by the dynamic MLC technique,'' Med. Phys. **25**, 1872–1879 (1998).
[28]W. Huang, L. E. Antonuk, J. Berry, M. Maolinbay, C. Martelli, P. Mody,

S. Nassif, and M. Yeakey, ''An asynchronous, pipelined, electronic acquisition system for active matrix flat-panel imagers (AMFPIs),'' Nucl. Instrum. Methods Phys. Res. A **431**, 273–284 (1999).

[29]K. L. Pasma, M. Kroonwijk, J. C. J. de Boer, A. G. Visser, and B. J. M. Heijmen, ''Accurate portal dose measurements with a fluoroscopic electronic portal imaging device (EPID) for open and wedged beams and dynamic multileaf collimation,'' Phys. Med. Biol. **43**, 2047–2060 (1998).

[30]A. S. Beddar, T. R. Mackie, and F. H. Attix, ''Water-equivalent plastic scintillation detectors for high-energy beam dosimetry. I. Physical characteristics and theoretical considerations,'' Phys. Med. Biol. **37**, 1883–1900 (1992).

[31]A. S. Beddar, T. R. Mackie, and F. H. Attix, ''Water-equivalent plastic scintillation detectors for high-energy beam dosimetry. II. Properties and measurements,'' Phys. Med. Biol. **37**, 1901–1913 (1992).